Journal of the Iranian Chemical Society (2018) 15:2649–2658
https://doi.org/10.1007/s13738-018-1453-5

ORIGINAL PAPER

Preparation of two-color photoluminescence emission based on azo dye-layered double hydroxide systems and controlling photoluminescence properties of Allura Red AC

Leila Jafari Foruzin[1] · Zolfaghar Rezvani[1] · Kamellia Nejati[2]

Received: 10 July 2017 / Accepted: 14 July 2018 / Published online: 21 July 2018

Abstract
The purpose of the present study was to synthesize types of organic–inorganic hybrid photofunctional materials and also to control their photoluminescence properties. Furthermore, we reported synthesis of a nanohybrid with two-color blue/violet and two-color red/yellow photoluminescence (PL) using the photofunctional anion (Allura Red AC) and Mg–Al-layered double hydroxide (LDH) nanosheets as the basic building blocks. The detailed chemical structure of the obtained composites was characterized by X-ray diffraction and infrared spectra (FT-IR). The results confirmed that Allura Red AC was successfully intercalated into the interlayer space of LDHs and the Allura Red AC–Mg_3Al-LDH and Allura Red AC–Zn_3Al-LDH hybrids were obtained with interesting photoemission properties. The PL analysis and diffuse reflectance spectroscopy (DRS) were used to study the photophysical properties. Allura Red AC–LDH systems exhibited a blue shift photo emission compared with the pristine Allura Red AC sample. Furthermore, Allura Red AC–Mg_3Al-LDH exhibited superior photoluminous efficiency with a dual-color emission, while Allura Red AC and Allura Red AC–Zn_3Al-LDH were one-color systems. Decreased band gap energy of Allura Red AC–LDH which is lower than that of Allura Red AC caused improved conductivity properties. Moreover, it was found from the DRS results that Allura Red AC–LDH could be regarded as the adsorbent electromagnetic wave and as a cover to protect materials against the electromagnetic waves. Therefore, this work provided a facile way for fabricating nanohybrids with two-color PL and controlling photoluminescent properties of the nanohybrids which had potential applications in the area of photoluminescent materials.

✉ Kamellia Nejati
nejati_k@yahoo.com; k_nejati@pnu.ac.ir

[1] Department of Chemistry, Faculty of Basic Sciences, Azarbaijan Shahid Madani University, Tabriz, Iran

[2] Department of Chemistry, Payame Noor University, P.O. Box 19395-3697, Tehran, Iran

Graphical abstract

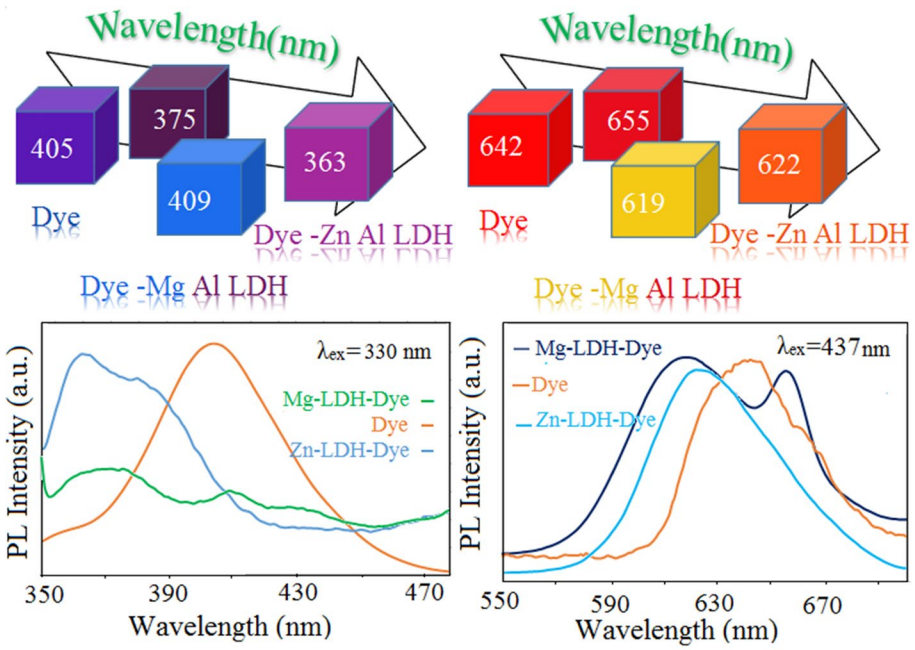

Keywords Allura Red AC–layered double hydroxide · Photoluminescence · H-type aggregation · Blue shift photoemission · Two-color emission

Introduction

Azo dyes are applied in lasers, light tones, solid-state self-emission devices, and sensors due to their broad spectra, strong fluorescence intensity, and high quantum yield [1–3]. In addition, synthesis of inorganic materials that directly make light from a solid material has received considerable attention [4]. When these dyes adjoin inorganic materials, nanohybrids, which have interesting photoluminescent properties, are made. Such materials, due to their photoluminescent properties, can be applied as batteries [5] in devices used for energy storage [6], electronic devices [7], sunscreen systems [8], drug carriers [9], and photofunctional materials [10]. On the other hand, azo dyes also have limited applications in optic fields, since the organic dyes are unstable under the environmental conditions such as high temperature, sunlight, and oxygen, which severely limit their applications in the pigment and optic industry [11–13]. Therefore, organic dyes should be attached to various supports such as silica [14] and polymers [15] or they can intercalate into layered double hydroxides [16] and so forth.

The two-dimensional layered double hydroxide (LDH) including a positively charged metal hydroxide layer, counter anions, and water molecules placed in the interlayer spaces is widely used as the host inorganic material to intercalate dye molecules onto the LDH matrix. The general formula of LDH can be described as $[M_{1-x}^{2+} M_x^{3+} (OH)_2]^{x+} [(A^{n-})_{x/n} \cdot nH_2O]^{x-}$, where A^{n-} is the charge balancing anion of valence *n*, *x* is at the range of 0.2 to 0.33 in $x = M^{3+}/(M^{2+} + M^{3+})$, and M^{2+} and M^{3+} are the divalent and trivalent metal cations occupying the octahedral holes of the brucite-like layers [17, 18]. The divalent metal cations undergo isomorphous substitutions by trivalent metal cations of the hydroxide layers, resulting in positive net charges that are electrically balanced by the A^{n-} anion in the interlayer spaces. Using anion exchange or intercalation reactions could place several varieties of anions into the interlayer spaces of LDH and prepare a new organic–inorganic hybrid LDH with unique and suitable properties [19]. LDHs have also been applied as inorganic hosts for intercalation of the organic dyes to fabricate organic–inorganic hybrid materials, which have potential applications in the area of optical functional devices and pigments. A lot of researches have been published on organic dye-intercalated LDHs such as anionic azo-type dyes [20–22], fluorescein anions [23, 24], perylene derivatives [25], and anionic anthracene type dyes. Controlled organization of the fluorescent organic dyes in a solid matrix offers numerous prospective applications in the field of chemical and biological sensing technologies. Some studies showed that the organic dye anion-LDH

systems have a blue or red shift photoemission and improved fluorescent performance compared to the pristine azo dye sample [26–29]. The ordered structures and surface charges of the LDH could effectively provide defined microscopic environments, a tunable loading density, and photo stability to the fluorescent organic dyes [30, 31]. Using intercalation of azo dyes as the guest anions in LDHs can prepare tunable solid-state lasers [32]. Moreover, intercalation reaction is a useful way to protect azo dyes from decomposition at high temperature, oxidation, and photo-degradation [10]. Therefore, a layered double hydroxide is a nano vessel in which inorganic, organic, and organometallic molecules and even polymers, which are preserved and withdrawn after a chemical reaction [33], may exist. Thus, it is possible to improve and control photoluminescent properties of azo dyes with high stability under high temperature and sunlight by making sandwich structures with inorganic matrixes. One of the important challenges in the field of optical physics is building materials with a two-color photoemission. Materials with two-color and multi-color PL emissions are still rather rare. Particularly, it is still difficult to obtain nanohybrid materials with a two-color emission, using azo dyes which themselves have one-color PL. Materials such as these substances can have important and new applications in the field of sensor and optical devices. This inspires us to create and develop new types of functional molecule-based optoelectronic materials. One of the azo dyes which has photoluminescent properties is Allura Red AC (Scheme 1). It seems that hybrids containing this dye and prepared by intercalation in layered double hydroxides (LDHs) have high environmental stability with useful photoluminescent properties such as blue shift at Allura Red AC–Zn_3Al-LDH and Allura Red AC–Mg_3Al-LDH compared to Allura Red AC. While Allura Red AC–Mg_3Al-LDH shows two-color PL, Allura Red AC has a one-color emission. Synthesis of these materials is necessary in fabrication of the solid-state dye laser and dye-based molecular optical devices. Allura Red AC–LDH materials have advantages of facile manipulation, low-cost, and environment-friendly lines and using this material facilitates realization of the optical/chemical sensors with rapid response and recyclability. Therefore, this work provides a viable method for controlling photoluminescence emission of Allura Red AC and fabricating a nanohybrid with two-color photoluminescence emission based on the low cost and facile incorporation of azo dye into LDHs. In this work, we reported preparation of Zn–Al and Mg–Al hydrotalcite intercalated with the Allura Red AC anions by the co-precipitation method using zinc and magnesium as the bivalent cations, aluminum as the trivalent cation, and dye as the anion. A detailed study of the structure of the LDHs and Allura Red Ac anion using several analyses such as FT-IR and X-ray diffraction approved that Allura Red Ac was placed into the layered double hydroxide and a two-color photoluminescence nanohybrid can also be obtained. Size and morphology of the final products were investigated by the scanning electron microscopy (SEM) images. Photoluminescence (PL) was used to study the optical property. The diffuse reflectance spectroscopy (DRS) technique was used to verify the electronic structure of the azo dye-LDH system.

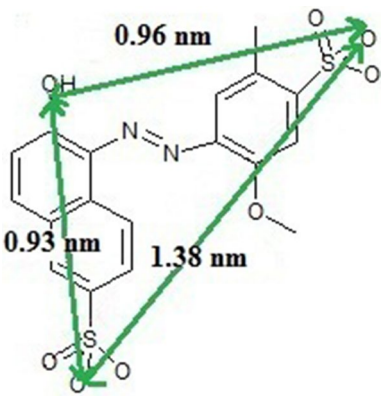

Scheme 1 The chemical structure of Allura Red AC

Experimental

Materials

$Zn(NO)_3{\cdot}6H_2O$, $Mg(NO)_3{\cdot}6H_2O$, $Al(NO)_3{\cdot}9H_2O$ and sodium hydroxide (NaOH pellets) were purchased from Sigma-Aldrich. Allura Red AC, an azo anionic dye, was obtained from Merck Company and used as received without further purification. Carbonate-free (de-CO_2) water was used throughout the experimental processes.

Syntheses of Allura Red AC–Zn_3Al-LDH and Allura Red AC–Mg_3Al-LDH

Allura Red AC anion-intercalated Mg_3Al-LDH and Zn_3Al-LDH were prepared with the co-precipitation method under nitrogen atmosphere. For theoretical 100% anion exchange, a solution containing Allura Red AC (0.296 g, 0.0006 mol) was slowly added to an aqueous mixed solution (20 mL) of $Zn(NO_3)_2{\cdot}6H_2O$ (0.849 g, 0.003 mol) [or $Mg(NO_3)_2{\cdot}6H_2O$ (0.769 g, 0.003 mol)] and $Al(NO_3)_3{\cdot}9H_2O$ (0.375 g, 0.001 mol). Afterward, the solution pH was adjusted to 9.5 by drop wise adding of NaOH. The resultant precipitate was maintained for 72 h at 70 °C. Then, the red product was centrifuged and washed with water three times. The obtained Allura Red AC–LDH was dried at room temperature.

Characterizations

Powder X-ray diffraction patterns (PXRD) of Allura Red AC–LDH were conducted with a Bruker AXS model D8 Advance diffractometer under the following conditions: Cu-K_α radiation ($\lambda = 1.54$ Å) at 40 kV and 35 mA with a Bragg angle ranging from 4° to 70°. Fourier transform infrared spectra (FT-IR) were recorded in the range of 3750–400 cm^{-1} with the KBr disk technique using a Perkin-Elmer spectrophotometer. The morphology of the samples was obtained by scanning electron microscope (SEM, Tescan Miea3) on the Au-coated samples using a Philips device (model XL30). Diffuse reflectance spectroscopy (DRS) was measured by absorbance ranging from 300 to 1000 nm on the Firmware Version: 061020 Software Version: Lab Pro Plus Build 410.1. The photoluminescence emission spectra of the samples were recorded using a JASCO luminescence spectrometer with the excitation wavelength of 330 and 437 nm. The thermogravimetric analysis (TGA) and differential thermal analysis (DTA) were recorded on the Linseis STA PT-1000 device with the heating rate of 10 °C min^{-1} in nitrogen atmosphere. The elemental CHN and metal ion content analyses of the resulting materials were carried out by Thermo Finnigan Flash EA 1112 Elemental Analyzer and ICP-OES (Perkin-Elmer, P-1000) spectrometer, respectively.

Results and discussion

The structural characterization of Allura Red AC–Zn_3Al-LDH and Allura Red AC–Mg_3Al-LDH

X-ray diffraction patterns

Figure 1 shows crystalline-layered phases of the precursor and Allura Red AC-intercalated LDHs. The XRD patterns of Zn_3Al–NO_3-LDH and Mg_3Al–NO_3-LDH (Fig. 1a in A, B) and Allura Red AC–Zn_3Al-LDH and Allura Red AC–Mg_3Al-LDH (Fig. 1b in A, B) showed that the crystals can be indexed for a hexagonal symmetry, with the space group of $R\bar{3}m$ which is commonly used to describe the 3R-type LDH [23, 34]. As shown in Fig. 1a in A and B, the basal spacing value, $d_{003,}$ which represents summation of the thickness of the brucite-like layer (0.48 nm) and the gallery height, is approximately 0.74 nm and 0.76 nm at Zn_3Al–NO_3-LDHs and Mg_3Al–NO_3-LDHs, respectively. They are consistent with those of nitrate-intercalated LDHs. Figure 1b indicates the XRD patterns of the intercalated Allura Red AC–LDHs (A and B). The main characteristic diffraction peaks of Allura Red AC–Zn_3Al-LDH appear at 5.16° ($d_{003} = 2.1$ nm), 9.24 ($d_{006} = 1.1$ nm), 13.20 ($d_{009} = 0.74$ nm), and 16.80 ($d_{012} = 0.55$ nm) and those of Allura Red AC–Mg_3Al-LDH appear at 4.05° ($d_{003} = 2.1$ nm), 8.24 ($d_{006} = 1.1$ nm), 12.20 ($d_{009} = 0.73$ nm), and 17.10 ($d_{012} = 0.52$ nm), respectively. During intercalation of the Allura Red AC molecules and replacing NO_3^- ions, the basal reflection (003) of the dye-LDH composites, in comparison with the precursor LDH, shifted to the lower 2θ angles and basal spacing of LDH increased from 0.74 to 2.1 nm at Allura Red AC–Zn_3Al-LDH and from 0.76 to 2.1 nm at Allura Red AC–Mg_3Al-LDH, respectively. The observed gallery height of 2.1 nm in dye-LDHs suggested that the Allura Red AC molecules with van der Waals radius of 1.38 nm (determined by the Chem Sketch software) were intercalated as the vertical and monolayer arrangements within the interlayers [1, 26].

The average crystallite size (D) of Mg_3Al-LDH, Zn_3Al-LDH, Allura Red AC–Zn_3Al-LDH, and Allura Red AC–Mg_3Al-LDH is calculated by employing Scherrer's formula :

$$D = 0.9\ \lambda / \beta \cos(\theta), \quad (1)$$

where D is the crystallite size (in nm), λ is the wavelength of the X-ray used (in nm), β is the full width at half maximum

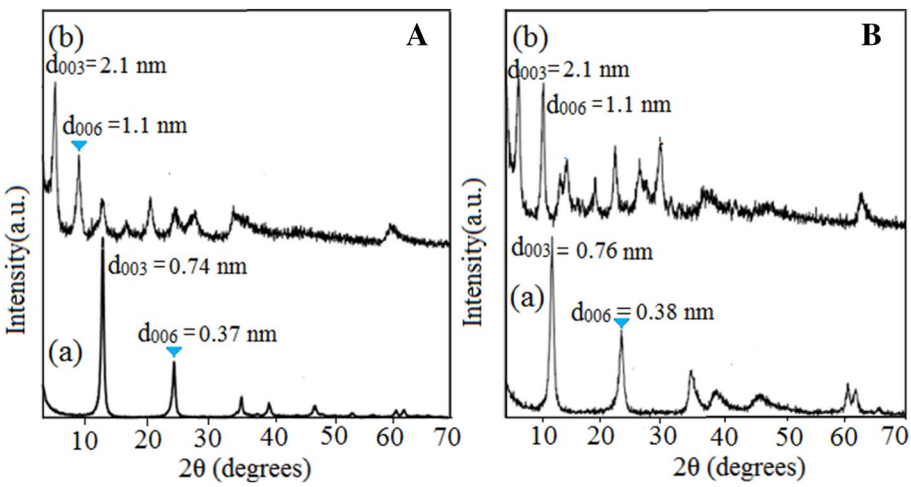

Fig. 1 The PXRD patterns of **A** [(a) Zn_3Al–NO_3-LDH, (b) Allura Red AC–Zn_3 Al-LDH)] and **B** [(a) Mg_3Al–NO_3-LDH, (b) Allura Red AC–Mg_3Al-LDH)]

(FWHM-in radian), and θ is the Bragg diffraction angle (in degree). The average crystallite size, D, was calculated 8.2, 8.7, 13.86, and 13.86 nm for Mg_3Al-LDH, Zn_3Al-LDH, Allura Red AC–Zn_3Al-LDH, and Allura Red AC–Mg_3Al-LDH, respectively.

FT-IR spectrum

The intercalation process and synthesis of Allura Red AC–Zn_3Al-LDH and Allura Red AC–Mg_3Al-LDH were also approved by the infrared spectroscopy. Figure 2A, B (a–c) shows the FT-IR spectra of LDHs and the Allura Red AC and Allura Red AC–LDH nanocomposites, respectively.

As shown in Fig. 2A (a), B (a), absorption peaks at 1359 and 1380 cm^{-1} can be ascribed to the ν_3 vibration of NO_3^- in the LDHs [35]. The wide and strong bands at 3440 and 3450 cm^{-1} correspond to the stretching vibrations of the hydroxyl groups that are placed at the surface and interlayer of the LDH [36], while the frequency of the stretching vibrations of the hydroxyl groups in free water is larger than this (3600 cm^{-1}). This is due to existence of the hydrogen bonding between the interlayer hydroxide groups and water of the layers. The two bands at 1627 and 1637 cm^{-1} were assigned to the bending vibration of the water molecules [34]. The peaks at 424 and 617 cm^{-1} are assigned to the vibration bands of Al–O and Zn–O (Fig. 2A (a). These values changed to 447 and 670 cm^{-1} at Al–O and Mg–O in Fig. 2B (a) [37, 38].

In case of pure Allura Red AC (Fig. 2A, B (b)), the strong absorption band at 3385 cm^{-1} is correlated with the stretching vibrations of the OH groups. Furthermore, the 1619 cm^{-1} peak is the vibration of C=C in the aromatic rings. The characteristic absorption band at 1369 cm^{-1} corresponds to the S=O asymmetric stretching vibrations of the sulfonate groups and the stretching vibration band of the N=N azo group appears at 1498 cm^{-1} [39]. After intercalation of the Allura Red AC molecules, the NO_3 bands at 1385 and 1380 cm^{-1} disappear; this indicates successful attachment of the Allura Red AC anions to the LDH nanoparticles. Additionally, it can be observed that the band vibrations of—SO_3^- in Allura Red AC–Zn_3Al-LDH and Allura Red AC–Mg_3Al-LDH, compared to the free—SO_3H in Allura Red AC, moved slowly to lower wave numbers (from 1369 to 1360 cm^{-1}) [40], suggesting the existence of two electrostatic and hydrogen bondings in the interlayer space.

The SEM images

Figure 3a, b present scanning electron microscopy (SEM) images of the Allura Red AC–Zn_3Al-LDH and Allura Red AC–Mg_3Al-LDH nanohybrids. Figure 3a shows that Allura Red AC–Zn_3Al-LDH is composed of aggregation of the irregular semi-bullet-like nanoparticles with the average size in the range of 26 nm. This figure reveals that they have a rough surface and they are composed of randomly oriented LDH particles with the pellet thickness of approximately 34 nm. The SEM image of Fig. 3b clearly shows the plate-like characteristic of the Allura Red AC–Mg_3Al-LDH nanohybrid. The SEM images of the Zn_3Al-LDH and Mg_3Al-LDH were given in supplementary Figures S_1 (a and b).

Thermal stability of the Allura Red AC–LDH nanohybrids

The TGA and DTA curves of the Allura Red AC dye and Allura Red AC–Mg_3Al-LDH and Allura Red AC–Zn_3Al-LDH nanohybrids are depicted in Fig. 4. For the pure Allura Red AC dye, two main weight losses are observed (Fig. 4a). The first one occurred in the temperature range of 50–200 °C (3.68%) caused by the evaporation of physically adsorbed water, accompanied by an endothermic DTA peak at 50 °C [25]. The other weight loss occurred in the temperature range of 200–700 °C, attributed to decomposition of the Allura Red AC dye (33%). This is confirmed by the

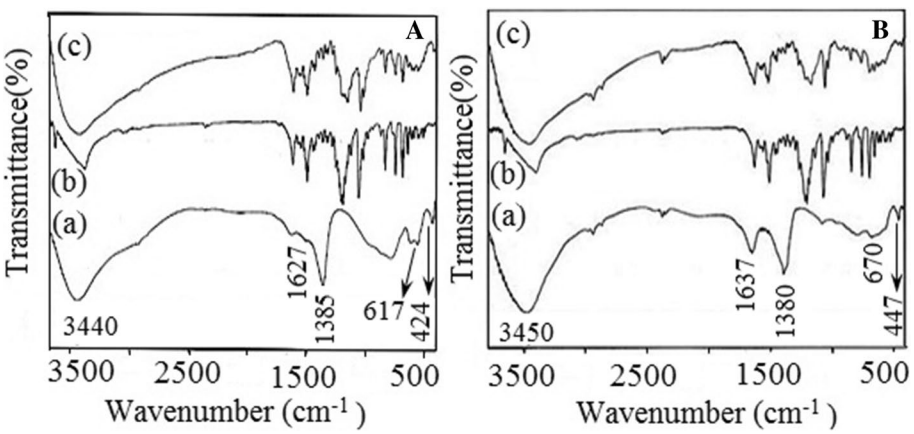

Fig. 2 FT-IR spectra of **A** [(a) Zn_3Al–NO_3-LDH, (b) Allura Red AC, (c) Allura Red AC–Zn_3Al-LDH] and **B** [(a) Mg_3Al–NO_3-LDH, (b) Allura Red AC, d] Allura and (c) Allura Red AC–Mg_3Al-LDH

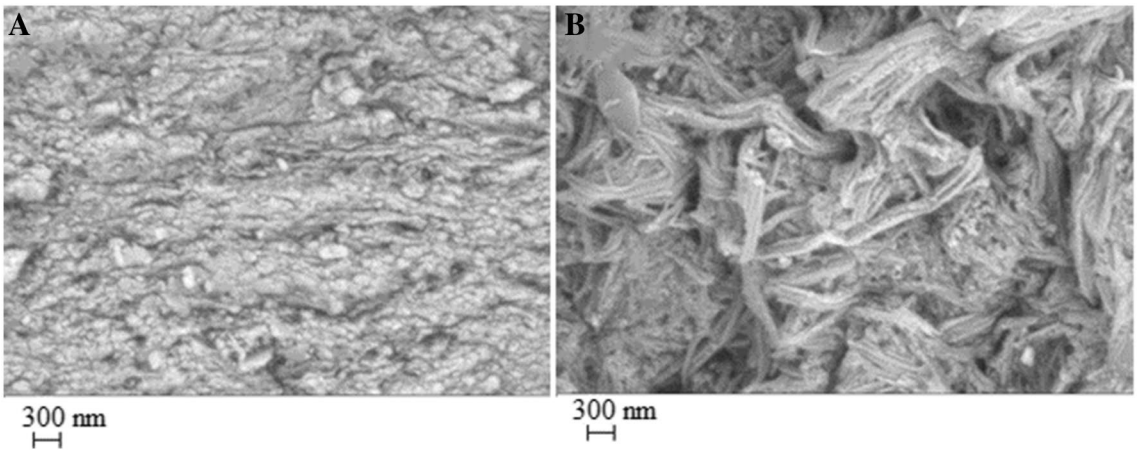

Fig. 3 The SEM images of **a** Allura Red AC–Zn_3Al-LDH, **b** Allura Red AC–Mg_3Al-LDH

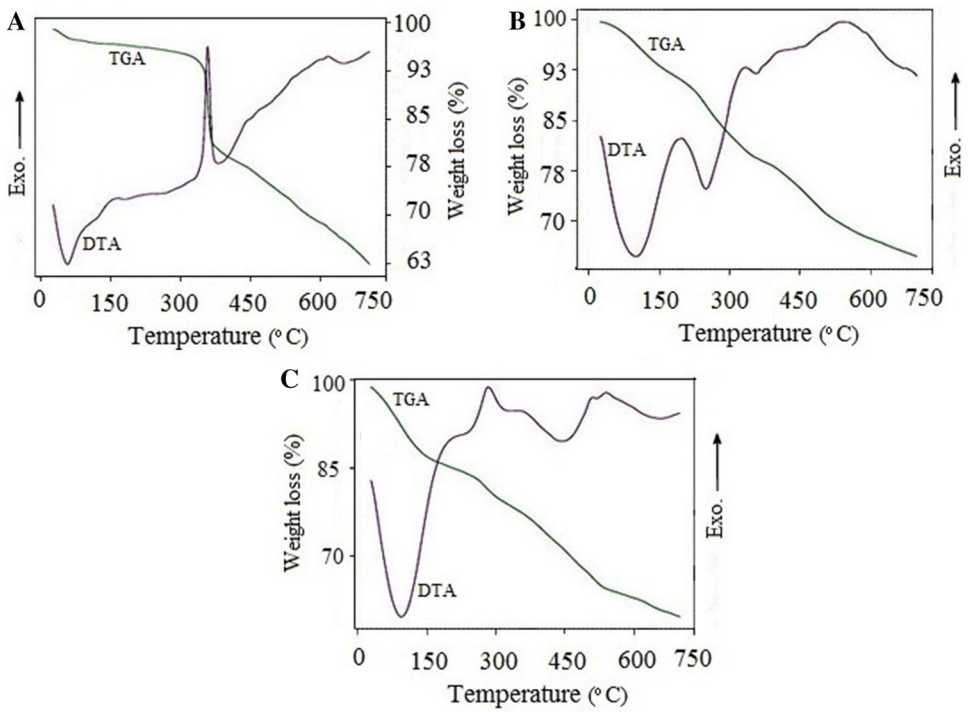

Fig. 4 The TG–DTA curves of **a** Allura Red AC, **b** Allura Red AC–Zn_3Al-LDH, and **c** Allura Red AC–Mg_3Al-LDH

appearance of a broad exothermic peak at 350 °C in the DTA curve correspondingly.

By comparison, the TGA curve of Allura Red AC–Zn_3Al-LDH shows three noticeable thermal events (Fig. 4b). The first main weight loss with two endothermic peaks (100 and 250 °C) occurred at 50–250 °C (9.74%). It is mainly due to evaporation of adsorbed and interlayer water. The next mass loss (250–350 °C) is attributed to dehydroxylation of the hydroxide layer (10.45%) while the exothermic peak of DTA appeared at 340 °C [40]. The last step (350–700 °C) which is accompanied with an exothermic peak at 550 °C was mostly resulted from the strong combustion of intercalated Allura Red AC (14.82%). As shown in Fig. 4c, the weight loss of Allura Red AC–Mg_3Al-LDH can be characterized by three steps. In the first step (50–150 °C), water is removed (12.35%); here, the endothermic peak of DTA appears at 100 °C and the trace of dehydroxylation in the LDH layer occurs at 150–300 °C whose exothermic DTA peak appeared at 300 °C (6.15%). The next weight loss (300–700 °C) with a strong DTA band centered at 550 °C corresponds to the decomposition or combustion of Allura Red AC as the organic guest (20.49%). All these temperatures are higher than the decomposition temperature of pure Allura Red AC; this demonstrates that the thermal stability of the intercalated Allura Red AC molecule enhanced.

Elemental analysis

Element chemical analyses of Mg, Zn, Al, C, N, and H for the prepared solids as well as their composition and molar ratios are summarized in Table 1. The results confirm that nitrate anions in the precursor were replaced by the Allura Red AC anions. The molar ratios of the metal ions in Allura Red AC–Zn_3Al-LDH and Allura Red AC–Mg_3Al-LDH are 3.2 and 2.97, respectively.

The nitrogen values found for Allura Red AC–Zn_3Al-LDH and Allura Red AC–Mg_3Al-LDH are almost the same as the calculated value. This confirmed that all of the nitrate anions replaced at Allura Red AC–LDHs and no nitrate anion was found at Allura Red AC–LDHs.

From these values, the approximate Allura Red AC loading into ZnAl-LDH and MgAl-LDH was determined to be around 31.58 and 38.32%, respectively. These values are less than those obtained from the TGA curves (Fig. 4b, c). Thus, these data confirmed that at 700 °C, the main part of Allura Red AC which intercalated into LDHs does not become decomposed due to an increase in the stability temperature of Allura Red AC–Zn_3Al-LDH and Allura Red AC–Mg_3Al-LDH.

Photophysical properties

Photoluminescence behavior

In this section, the PL emission spectra of the Allura Red AC dye and Allura Red AC–LDHs are investigated in the excitation wavelengths of 330 and 437 nm with dispersing Allura Red AC, Allura Red AC–Zn_3Al-LDH, and Allura Red AC–Mg_3Al-LDH in water (Fig. 5a, b). Comparing the PL properties of the pure dye and dye-LDHs shows that the fluorescent dye–LDH materials exhibited a red or blue shift compared to the dye solution only [41, 42] due to H-type (face-to-face) and J-type (tail-to-tail) arrangements of dye molecules in the interlayers of LDH. The blue or red shifts in the photoemission property can be controlled with these arrangements.

In Allura Red AC, the symmetrical emission peak can be observed at 405 nm when the excitation wavelength is 330 nm. Moreover, the emission peaks of Allura Red AC–Zn_3Al-LDH and Allura Red AC–Mg_3Al-LDH appeared at 363, 375, and 409 nm, respectively (Fig. 5a). When the excitation wavelength is 437 nm, the peaks of Allura Red AC–Zn_3Al-LDH appear at 622 nm and those of Allura Red AC–Mg_3Al-LDH appear at 619 and 655 nm (Fig. 5b). The blue shift of the spectrum of the Allura Red AC–Zn_3Al-LDH and Allura Red AC–Mg_3Al-LDH samples is due to formation of the H-type (face-to-face arrangement) aggregation in the LDH layers. The results obtained from XRD also

Table 1 Elemental chemical analyses' results for Allura Red AC–Zn_3Al-LDH and Allura Red AC–Mg_3Al-LDH

Sample	Zn	Mg	Al	C	H	N	Composition
Allura Red AC–Zn_3Al-LDH	38.8 (30.3)[a]	–	5 (4)	16.4 (16.6)	2.6 (3.3)	2.2 (2.1)	$Zn_{3.84}Al_{1.19}(OH)_8(C_{18}H_{14}N_2O_8S_2)_{0.49}.3.5H_2O$[b]
Allura Red AC–Mg_3Al-LDH	–	12 (14)	4.5 (5.0)	20.1 (20.5)	3.6 (4.2)	3.1 (2.7)	$Mg_{2.62}Al_{0.88}(OH)_8(C_{18}H_{14}N_2O_8S_2)_{0.48}.3.6H_2O$[b]

[a]Values given in parentheses correspond to theoretical values

[b]The amount of water at the stoichiometry formula was obtained from the TGA curves (Fig. 4 (b and c))

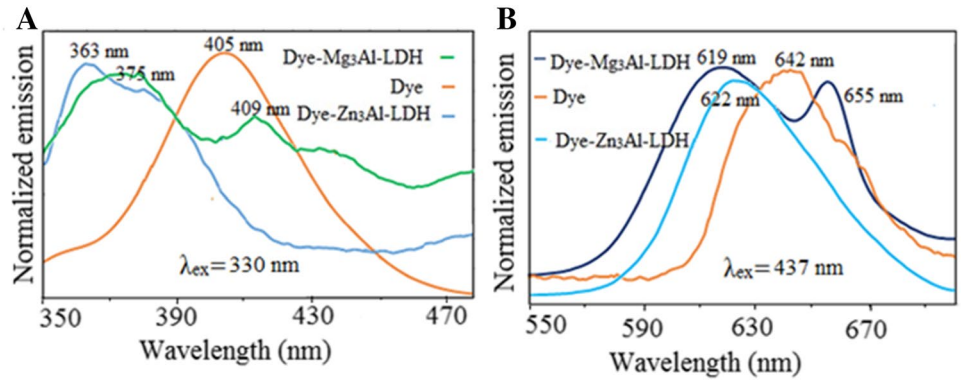

Fig. 5 **a, b** The photoluminescence (PL) emission spectra of Allura Red AC, Allura Red AC–LDHs, and LDHs which dispersed in water

confirm vertical arrangement of the Allura Red AC anions at the LDH layer. The photoluminescence (PL) behavior is related to transference of the photo-induced electrons and holes, which shows the separation–recombination process of the photo-induced charge carriers. The strongest PL emission peaks of the Allura Red AC dye appear at 405 and 642 nm, which are due to the excitation wavelengths of 330 and 437 nm, respectively. The strong emission peaks show the low rate of electron–hole recombination in the Allura Red AC azo dye, which had high photocatalytic properties [43]. The weak emission intensities of Allura Red AC–Zn_3Al-LDH and Allura Red AC–Mg_3Al-LDH with blue shifts, compared to Allura Red AC, exhibit a high rate of electron–hole recombination and stabilization of the Allura Red AC molecules in the LDH layer against light. Additionally, the Allura Red AC–Mg_3Al-LDH system exhibits a dual-color emission and a blue shift in the fluorescence of Allura Red AC (Fig. 5a, b). It seems that an amount of energy transferred from dye to Mg and this energy is responsible for generating a band at 409 and 655 nm [44, 45]. Therefore, in this work, with intercalation of the photoactive anions into LDH, we can synthesize low-cost LDHs with two-color luminescence and high stability using a facile method. The PL emission spectra of the Zn_3Al-LDH and Mg_3Al-LDH are given in supplementary Figures S_2 (a and b). Zn_3Al-LDH and Mg_3Al-LDH show the PL emission peaks at 420 and 400 nm which are attributed to the excitation wavelength of 330 nm. The emission peaks of Zn_3Al-LDH and Mg_3Al-LDH at 662 nm are related to the excitation wavelength of 437 nm. In both excitation wavelengths, the Allura Red AC–Zn_3Al-LDH and Allura Red AC–Mg_3Al-LDH systems exhibit a lot of blue shifts in comparison with pure LDH. The emission intensity of LDHs is extremely weaker than Allura Red AC–LDHs.

Diffuse reflectance spectroscopy (DRS)

Figure 6a shows the diffuse reflectance spectroscopy (DRS) of the products at room temperature. Compared with Allura Red AC, Zn_3Al-LDH, and Mg_3Al-LDH, a red shift was observed for the Allura Red AC–LDH nanocomposites; this can be attributed to an increase in aggregation of Allura Red AC at Zn_3Al-LDH and Mg_3Al-LDH [35]. Therefore, charge transfer of the sulfonate group of Allura Red AC to the metals of the LDHs caused a red shift in DRS. The spectra of Zn_3Al-LDH and Mg_3Al-LDH exhibit weak UV absorption between 300 and 350 nm due to the shielding effect of the LDH layers. After intercalation, Allura Red AC–Zn_3Al-LDH and Allura Red AC–Mg_3Al-LDH show an extraordinary absorption ability between 300 and 850 nm, which is stronger than LDH and Allura Red AC, and is correlated with the interactions between the guest and host layers. Thus, Allura Red AC–Zn_3Al-LDH and Allura Red AC–Mg_3Al-LDH can adsorb an amount of electromagnetic waves, and due to this property, they can be applied for protection against the electromagnetic wave. The optical bandgap energy, E_g, of Allura Red AC, Zn_3Al-LDH, Mg_3Al-LDH, Allura Red AC–Zn_3Al-LDH, and Allura Red AC–Mg_3Al-LDH were calculated by UV–Vis–DRS (Fig. 6a) and E_g of the samples was calculated using the following Tauc's equation:

$$\alpha = \frac{a_0(h\nu - E_g)^n}{h\nu}, \tag{2}$$

where a is the absorption coefficient, $h\nu$ is the photon energy, and α_0 and h are the constants [46]. As represented in Fig. 6b, the experimental values of the band gap energy determined for Allura Red AC, Allura Red AC–Zn_3Al-LDH, and Allura Red AC–Mg_3Al-LDH are $E_g = 2.01$, 1.87, and 1.75 eV, respectively. These results show that the band gap energy decreased with intercalation of Allura Red AC into LDH, causing enhanced conductivity of the dye. As shown in Fig. 6b, due to intercalation of an onion at the interlayer of LDH, which is larger than nitrate, these band gaps are lower than those of Zn3Al-LDH and Mg_3Al-LDH. The band gaps at Zn_3Al-LDH and Mg_3Al-LDH are 3.84 and 3.62 eV, respectively. Therefore, the band gap energy of the Allura Red AC–Zn_3Al-LDH and Allura Red

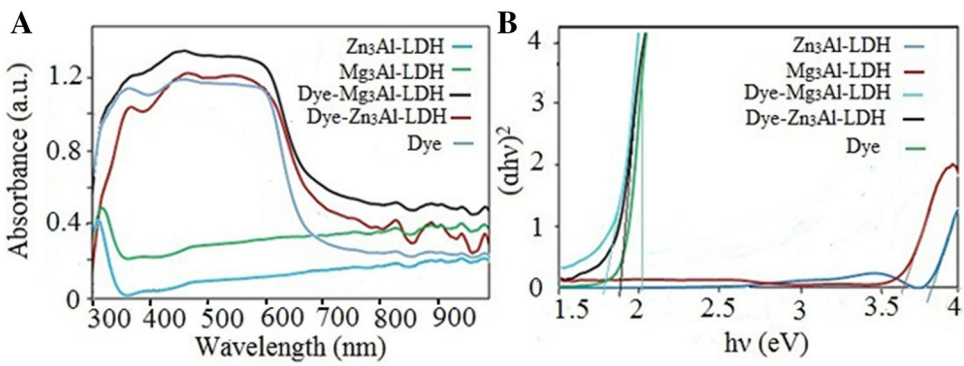

Fig. 6 **a** The diffuse reflectance spectroscopy (DRS)-UV–visible absorption spectrum of Allura Red AC–Zn_3Al-LDH, Allura Red AC–Mg_3Al-LDH, and Allura Red AC and **b** Tauc's plot for Allura Red AC–Mg_3Al-LDH, Allura Red AC–Zn_3Al-LDH, and Allura Red AC

AC–Mg_3Al-LDH molecules is lower than those of Allura Red AC, Zn_3Al-LDH, and Mg_3Al-LDH.

Conclusion

As mentioned in the "Introduction", the first objective of this paper was to synthesize nanohybrids with two-color blue/violet and two-color red/yellow PL emissions using Mg–Al-layered double hydroxide (LDH) and photofunctional anion (Allura Red AC) with one-color PL emission. The second aim was to improve photostability and photophysical properties of the organic dye anions–LDH systems. Our research group was successful in achieving both of the goals. The Allura Red AC anion was incorporated into the ZnAl–NO_3-LDH and MgAl–NO_3-LDH matrixes by the co-precipitation method, respectively. It was approved from the results of XRD and FT-IR that Allura Red AC was intercalated into galleries of LDHs. Scanning electron microscopy (SEM) images confirmed that Allura Red AC–Zn_3Al-LDH and Allura Red AC–Mg_3Al-LDH were in nano size. To evaluate the preferential orientation of the interlayer, the Allura Red AC molecules, fluorescence, and DRS were employed and the structures of the Allura Red AC–LDHs composites were proposed. These results suggest that the H-type (face-to-face arrangement) aggregation of the Allura Red AC molecules in the space of the LDH interlayers improves and controls fluorescent property of Allura Red AC. It was found from the result of DRS that Allura Red AC–Zn_3Al-LDH and Allura Red AC–Mg_3Al-LDH adsorb electromagnetic waves. Since the band gap energy in the Allura Red AC–LDH nanohybrid is lower than that of Allura Red AC, conductivity properties of Allura Red AC–LDH are better than Allura Red AC. The photoluminescence (PL) analysis indicated that both of the products have blue shift wavelength emissions in comparison with the pristine dye. Allura Red AC–Mg_3Al-LDH has a two-color emission, while Allura Red AC has a one-color emission. Moreover, this work provides a facile method for immobilization and dispersion of organic dyes within a 2D inorganic matrix with the purpose of prospective application in photoluminescence materials.

Acknowledgements The authors would appreciate Azarbijan Shahid Madani University for supporting this work.

References

1. Z. Sun, L. Jin, W. Shi, M. Wei, D.G. Evans, X. Duan, Langmuir **27**, 7113 (2011)
2. T. Tanaka, S. Nishimoto, Y. Kameshima, J. Matsukawa, Y. Fujita, Y. Takaguchi, M. Matsuda, M. Miyake, J. Solid State Chem. **183**, 479 (2010)
3. S.-M. Xu, S.-T. Zhang, W.-Y. Shi, F.-Y. Ning, Y. Fu, H. Yan, RSC Adv. **4**, 47472–47480 (2014)
4. H. Shahroosvand, F. Nasouti, E. Mohajerani, A. Khabbazi, J. Lumin. **135**, 339 (2013)
5. K.-N. Jung, J.-H. Jung, W.B. Im, S. Yoon, K.-H. Shin, J.-W. Lee, ACS Appl. Mater. Interfaces **5**, 9902 (2013)
6. A.V. Murugan, T. Muraliganth, A. Manthiram, Chem. Mater. **21**, 5004 (2009)
7. B. Xiao, X. Wang, H. Huang, M. Zhu, P. Yang, Y. Wang, Y. Du, J. Phys. Chem. C **117**, 21303 (2013)
8. S.M.N. Mohsin, M.Z. Hussein, S.H. Sarijo, S. Fakurazi, P. Arulselvan, T.-Y.Y. Hin, Chem. Cent. J. **7**, 26 (2013)
9. M.Z. Hussein, N.S.S.A. Rahman, S.H. Sarijo, Z. Zainal, Int. J. Mol. Sci. **13**, 7328 (2012)
10. F.J. Quites, J.C. Germino, T.D.Z. Atvars, Colloids Surf. A **459**, 194 (2014)
11. S.-H. Hwang, S.-C. Jung, S.-M. Yoon, D.-K. Kim, J. Phys. Chem. Solids **69**, 1061 (2008)
12. S. Gago, T. Costa, J. Seixas de Melo, I.S. Goncalves, M. Pillinger, J. Mater. Chem. **18**, 894 (2008)
13. P. Liu, P. Liu, K. Zhao, L. Li, Opt. Laser Technol. **74**, 23 (2015)
14. M.P.B. van Bruggen, Langmuir **14**, 2245 (1998)
15. S. Lelu, C. Novat, C. Graillat, A. Guyot, E. Bourgeat-Lami, Polym. Int. **52**, 542 (2003)
16. P. Tang, X. Xu, Y. Lin, D. Li, Ind. Eng. Chem. Res. **47**, 2478 (2008)
17. Q. Wang, D. O'Hare, Chem. Rev. **112**, 4124 (2012)
18. H. Chen, L. Hu, M. Chen, Y. Yan, L. Wu, Adv. Funct. Mater. **24**, 934 (2014)
19. J.H. Lee, D.-Y. Jung, E. Kim, T.K. Ahn, Dalton Trans. **43**, 8543 (2014)
20. S. Mandal, D. Tichit, D.A. Lerner, N. Marcotte, Langmuir **25**, 10980 (2009)
21. P. Tang, F. Deng, Y. Feng, D. Li, Ind. Eng. Chem. Res. **51**, 10542 (2012)
22. G. Bascialla, A.E. Regazzoni, Colloids Surf. A **328**, 34 (2008)
23. D. Yan, J. Lu, J. Ma, M. Wei, D.G. Evans, X. Duan, Phys. Chem. Chem. Phys. **12**, 15085 (2010)
24. J. Bauer, P. Behrens, M. Speckbacher, H. Langhals, Adv. Funct. Mater. **13**, 241 (2003)
25. P. Tang, Y. Feng, D. Li, Dyes Pigments **104**, 131 (2014)
26. D. Yan, Y. Zhao, M. Wei, R. Liang, J. Lu, D.G. Evans, X. Duan, RSC Adv. **3**, 4303 (2013)
27. Z. Wang, F. Liu, C. Lu, Chem. Commun. **47**, 5479 (2011)
28. L. Zhang, Z. Zhang, C. Lu, J.-M. Lin, J. Phys. Chem. C **116**, 14711 (2012)
29. M. Zhang, D. Han, C. Lu, J.-M. Lin, J. Phys. Chem. C **116**, 6371 (2012)
30. U. Costantino, F. Costantino, F. Elisei, L. Latterini, M. Nocchetti, Phys. Chem. Chem. Phys. **15**, 13254 (2013)
31. L. Latterini, M. Nocchetti, G.G. Aloisi, U. Costantino, F. Elisei, Inorg. Chim. Acta **360**, 728 (2007)
32. C. Chakraborty, K. Dana, S. Malik, J. Phys. Chem. C **115**, 1996 (2011)
33. W. Shi, Z. Sun, M. Wei, D.G. Evans, X. Duan, J. Phys. Chem. C **114**, 21070 (2010)
34. Y. Zhao, J.-G. Li, F. Fang, N. Chu, H. Ma, X. Yang, Dalton Trans. **41**, 12175 (2012)
35. Z. Sun, L. Jin, W. Shi, M. Wei, X. Duan, Chem. Eng. J. **161**, 293 (2010)
36. Z. Zhang, G. Chen, K. Xu, Ind. Eng. Chem. Res. **52**, 11045 (2013)
37. S. Zheng, J. Lu, W. Li, Y. Qin, D. Yan, D.G. Evans, X. Duan, J. Mater. Chem. C **2**, 5161 (2014)
38. S.P. Lonkar, B. Kutlu, A. Leuteritz, G. Heinrich, Appl. Clay Sci. **71**, 8 (2013)
39. M. Asniza, A. Issam, H.A. Khalil, Sains Malays. **40**, 765 (2011)

40. L. Yang, L. Qian, Y. Feng, P. Tang, D. Li, Ind. Eng. Chem. Res. **53**, 17961 (2014)
41. E. Káfuňková, C. Taviot-Guého, P. Bezdička, M. Klementová, P. Kovář, P. Kubát, J. Mosinger, M. Pospíšil, K. Lang, Chem. Mater. **22**, 2481 (2010)
42. M. Jiřičková, J. Demel, P. Kubát, J. Hostomský, F. Kovanda, K. Lang, J. Phys. Chem. C **115**, 21700 (2011)
43. Y. Zhao, B. Li, Q. Wang, W. Gao, C.J. Wang, M. Wei, D.G. Evans, X. Duan, D. O'Hare, Chem. Sci. **5**, 951 (2014)
44. G. Li, D. Geng, M. Shang, Y. Zhang, C. Peng, Z. Cheng, J. Lin, J. Phys. Chem. C **115**, 21882 (2011)
45. K.H. Kwon, W.B. Im, H.S. Jang, H.S. Yoo, D.Y. Jeon, Inorg. Chem. **48**, 11525 (2009)
46. L.J. Foruzin, Z. Rezvani, K. Nejati, RSC Adv. **6**, 10912 (2016)